Transcriptomics reveal new insights into molecular regulation of nitrogen use efficiency in Solanum melongena

International Journal of Pavement Engineering

A study on the dependence of PEMs acoustic properties on incidence angle

F.G. Praticò,R. Vaiana &R. Fedele

Abstract. The objective of this paper is to study the variability of on-site acoustic measurements in non-normal conditions, as a function of the angle. A porous European mix was investigated. In order to reject the hypothesis that the cause of the variations in the acoustic properties is the surface inhomogeneity, texture properties were investigated according to the standard ISO 13473-1 and ISO/CD TS 13473-4. The acoustic absorption coefficient was measured according to ISO 13472-1. Results were compared and analysed in terms of averages and standard deviations. Result analyses may allow us to derive how absorption properties may vary as a function of the angle of incidence (under the hypothesis of homogeneous surface texture of the friction course). A tentative theoretical framework for explaining the dependence of acoustic absorption on incidence angle was formulated. The outcomes of this study are expected to benefit both practitioners and researchers.

Keywords: sound absorption properties; surface texture; angle of incidence; surface inhomogeneity; porous friction course.

Introduction

Porous European mixes (PEMs; air voids content, AV, usually in excess of 20%) act as a wearing course (often 50 mm thick) on impermeable base courses and have well-known advantages: reduction of splash and spray, mitigation of outdoor noise (high porosity, low flow resistivity), optimisation of skid resistance at high speeds in wet conditions (high macrotexture; Alvarez et al.2010, Praticò et al.2011, Praticò et al.2012a, 2012b, Praticò and Vaiana 2012) and waterstorm mitigation (Filianoti 2001).

In contrast, PEMs have several disadvantages: clogging, appreciable variation of volumetrics, noise, texture, friction, and permeability performance over the time.

Furthermore, permeability can affect moisture susceptibility (Kringos and Scarpas 2008).

PEM advantages in terms of noise mitigation are very important because noise pollution is one of the most important environmental problems in Europe (see European Commission 2002, Freitas et al.2012, Praticò and Anfosso 2012, Shen et al.2013). In more detail, noise reduction at the source is very cost-effective (more than treatments on the buildings or on the propagation path – noise barriers). Power unit and tyre–road contact are the main sources. In the mid-to-high speed ranges (approximately above 40 km/h for passenger cars and 70–80 km/h for trucks), the main contributor to traffic noise is tyre/road (rolling) noise (Sandberg and Ejsmont 2002). Pavement–tyre interaction generates acoustical pressures (Weyl–Van Der Pol's equation) which generate loudness (Attenborough 1983, Praticò 2001, Frías et al.2011, Jimenez-Espadafor et al.2011). Surface texture and absorption coefficient are the main inputs. To this end, it is noted that: (i) rolling noise (and generation factors in Weyl–Van Der Pol's equation) and acoustic absorption depend on surface texture and on porosity and (ii) in turn, porosity is correlated with the texture itself and many authors developed correlations between surface texture and air void content (Meegoda et al.2002, Boscaino et al.2009, Loprencipe and Cantisani 2013, Praticò and Vaiana 2013).

Several tools for experimental assessment can be listed. In situ methods are generally preferred and several methods are available for outdoor tyre/road noise measurements. These simple and robust methods are used to evaluate the noise performance of a road surface and possibly to label/classify it. The following acoustic noise performance indicators for road surfaces can be listed: (i) statistical pass by method (ISO 11819-1), (ii) controlled pass by method, (iii) close proximity method (ISO/CD 11819-2) and (iv) on board sound intensity (AASHTO TP76). Auxiliary measurement methods of noise-relevant surface characteristics are sometimes used (texture, sound absorption – ISO 13472-1, ISO 10534-1-2 – mechanical impedance or dynamic stiffness, for very elastic pavements, see Biligiri 2013). In more detail, the sound absorption coefficient indicates how much of the sound is absorbed in the actual material and several in situ methodologies can be listed (Londhe et al.2009): ISO 13472-2:2010 (only for reflective surfaces) and ISO 13472-1:2002 (extended surface or Adrienne method).

Note that by referring to the ISO 13472-1, the measurement in non-normal conditions is now required (ANAS 2008).
This contract requirement implies important consequences in terms of quality assurance, quality control, contract administration and theoretical approach (variation of the absorption coefficient as a function of the angle).
Furthermore, the results are not anymore comparable with Kundt-type measurements (ISO 10534-1:1996, ISO 10534-2:1998, ISO 13472-2:2010).
Note that to this end: (i) the setup of the device should permit a stable measurement in non-normal conditions and (ii) a theoretical framework is needed for the interpretation and prediction of the results.

Objective of the study

In the light of the abovementioned contract requirements, the objective of this paper is to study the variability of in situ acoustic absorption coefficient as a function of angle, for a given friction course.

In more detail, this study aims at assessing the dependence of the in situ absorption coefficient on the angle of incidence, as measured according to the standard UNI ISO 13472-1:2004. In order to reject the hypothesis that the cause of the variations of the acoustic properties is pavement inhomogeneity and to gather other information about the properties of the surface under investigation, texture properties were investigated according to the standard ISO/CD TS 13473-4.

Methodology

Absorption coefficient

The configuration of the probe during the measurements (normal incidence) according to the standard ISO 13472-1:2004 is shown in Figure 1 (see also Table A1 in

Appendix).

Figure 1 Configuration of the probe during the measurements (normal incidence). M, microphone; S, loudspeaker; R, centre of rotation of the probe (pivot); dr = 1.585 m (pivot height); dm = 0.25 m (microphone height); dRS = 0.335 m (height of the probe box); dSM = 1.00 m (loudspeaker-to-microphone distance).

The ISO 13472-1:2004 method (or Adrienne method, or extended surface method) is based on the recovering of an acoustic impulse response close to the pavement under test (Morgan and Watts 2003, Londhe et al.2009; Lin and Wang 2013).

A loudspeaker is placed facing the pavement and a microphone is placed between the sound source and the pavement.

With the loudspeaker emitting a transient sound, the microphone receives both the direct sound pressure wave travelling from the sound source to the pavement and the sound pressure wave reflected (including scattering) by the surface under test.

The power spectra of the direct and the reflected components, corrected to take into account the path length difference of the two components, give the basis for calculating the acoustic absorption coefficient.

In more detail, the pseudorandom maximum-length sequence (MLS) is continuously fed to the sound source which emits a sound signal modulated by the MLS. Note that other types of sound signal can be used (European Commission 1998; ISO 13471-1; Alvarez et al. 2012).

The sound absorption coefficient can be expressed as a function of the impulse responses through the following relationship:

$$\alpha(f) = 1 - \frac{1}{K_r^2}\left|\frac{H_r(f)}{H_i(f)}\right|^2 \qquad (1)$$

where Hr(f) is the transfer function of the reflected component impulse response, hr(t), that is obtained applying two techniques for data analysis to overall microphone response, i.e. signal subtraction technique (Mommertz 1995, Guidorzi and Garai 2008) and time windowing.

Hi(f) is the transfer function of the direct component impulse response, hi(t), that is obtained performing a free-field measurement with the same geometrical configuration of the setup. The transfer functions are obtained applying the fast Fourier transform (FFT) to each of the impulse responses.

The sound absorption coefficient can be also expressed as a function of the sound reflection factors through the following relation:

$$\alpha(f) = 1 - \left|Q_{p,road}(f)\right|^2 = 1 - \left|\frac{Q_{p,road,meas}(f)}{Q_{p,ref,meas}(f)}\right|^2 = 1 - \frac{Q_{W,road,meas}(f)}{Q_{W,road,ref}(f)} \quad (2)$$

where Qp,road(f) is the sound pressure reflection factor of the surface under investigation; Qp,road,meas(f) is the sound pressure reflection factor of the road surface under test measured in situ; QW,road,meas(f) is the sound power reflection factor of the road surface under test measured in situ and QW,road,ref (f) is the sound power reflection factor of the reference surface measured in situ.

Note that there are two types of sound reflection factors in the previous relation, i.e. the sound pressure reflection factor, Qp(f), and the sound power reflection factor, QW(f). The relationship between these sound reflection factors is:

$$Q_W(f) = \left|Q_p(f)\right|^2 \quad (3)$$

Note that in the case of normal incidence, the effective radius of the circular surface which is interested by the reflection is given by:

$$r = \frac{1}{d_s + d_m + c \cdot T_W} \cdot \sqrt{\left(d_s + d_m + \frac{c \cdot T_W}{2}\right) \cdot \left(d_s + \frac{c \cdot T_W}{2}\right) \cdot \left(2d_m + c \cdot T_W\right) \cdot c \cdot T_W} \quad (4)$$

where ds and dm are the respective heights above the test surface of the loudspeaker and the microphone, c is the speed of sound in air and Tw is the duration of the time window applied to the impulse response (UNI ISO 13472-1:2004).

As for c, an increase in T from 20 to 21°C increases c by 0.6 m/s and the following equation can be used:

$$c \cong 331.4 + 0.6 \cdot \tau \qquad (5)$$

where τ is the air temperature measured in situ, expressed in °C. Figure 1 illustrates the configuration of the probe (loudspeaker–microphone) during the measurements at normal incidence.

In the case of non-normal incidence (see Figure 2), the extended surface will be an ellipse and not a circle.

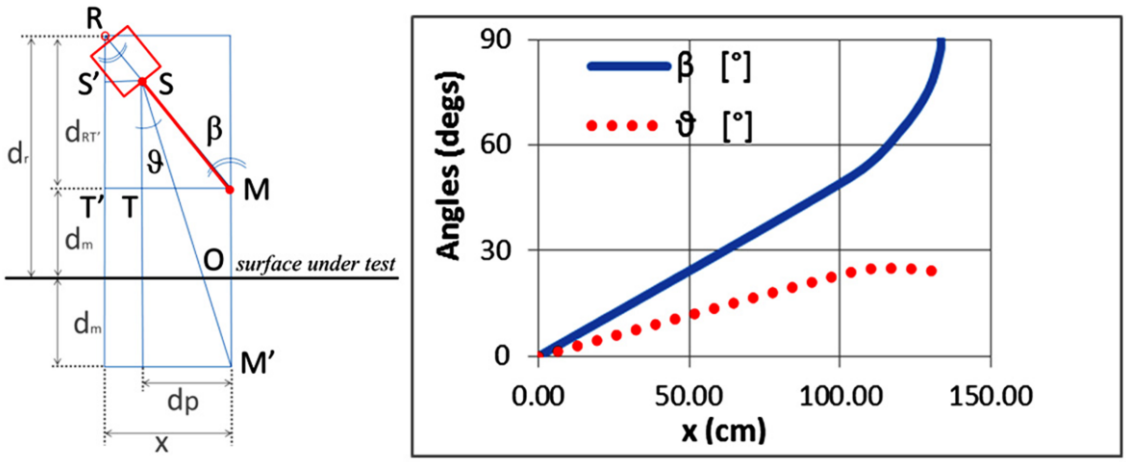

Figure 2 Non-normal measurements.

Legend of figure 2:

M = microphone probe; S = loudspeaker of the probe; R = center of rotation of the probe; β = rotation angle of the probe; θ = angle of incidence of the sound field; x = projection of the pivot-microphone distance; dp = projection of the loundspeaker-microphone distance; d_r = 1.585 m (pivot height); d_m= 0.25 m (microphone height); d_{RS} = 0.335 m (height of the probe box); $d_{RS'}$: vertical projection of d_{RS}; $d_{SS'}$: horizontal projection of d_{RS}; $d_{S'T'}$: vertical projection of d_{SM}; d_{TM}: horizontal projection of d_{SM}; d_{RM} = 1.335 m (probe length); d_{SM} = 1.00 m (loudspeaker-microphone distance).

The major axis of the ellipse will measure:

$$2a = cT_W + \sqrt{(d_s + d_m)^2 + d_p^2} \qquad (6)$$

where d_p is the projection on the pavement of the distance of the loudspeaker from the microphone if an incident angle ϑ is considered (see Figure 2), the factor of geometric divergence, $K_{r,\vartheta}$, is given by:

$$K_{r,\vartheta} = \frac{d(S,M)}{d(S,M')} = \frac{d(S,M)}{d(S,O,M)} \qquad (7)$$

Where S is the acoustic source, M is the receiver, M' is the image receiver, O is the object (surface under test), d(S, M) is the distance between S and M, while d(S, M') is the sum of the distance between S and O and the distance between O and M.

The distances *d(S, M)* and *d(S, O, M)* can be computed as follows:

$$d(S,O) = \left[\left(\frac{d_s + d_m}{\cot \vartheta} \right)^2 + (d_s - d_m)^2 \right]^{\frac{1}{2}} \qquad (8)$$

$$d(S,O,M) = \left(\frac{d_s + d_m}{\cos \vartheta} \right) \qquad (9)$$

It follows:

$$K_{r,\vartheta}^2 = 1 - \cos^2 \vartheta \left[1 - \left(\frac{d_s - d_m}{d_s + d_m} \right)^2 \right] \qquad (10)$$

Note that $K_{r,\vartheta}$ can be also expressed as follows:

$$K_{r,\vartheta} = 1 - \cos^2 \vartheta \left(1 - K_r^2\right) \qquad (11)$$

It follows that for a given incidence angle, ϑ, the absorption coefficient results:

$$\alpha_\vartheta(f) = 1 - \frac{1}{K_{r,\vartheta}^2} \left| \frac{H_{r,\vartheta}(f)}{H_{i,\vartheta}(f)} \right|^2 \qquad (12)$$

Where $H_{r,\vartheta}(f)$ is the transfer function (reflection) while $H_{i,\vartheta}(f)$ is another transfer function (direct path).

As is well known, the Adrienne system doesn't include a toll for fixing the probe in a direction exactly normal to the pavement surface.

Furthermore, several contract specifications (ANAS 2008) require an angle of 30° (it is supposed that they refer to the angle β). It can be supposed that this requirement is due to the need of better simulating the phenomena which happen between the car and the pavement.

If the angle between the loudspeaker-to-microphone direction and pavement is different from 90°, then the problem can be analysed by using equations 13 to 23 (see Figs.1-3).

In Figs 1 an d 2, d_{RS} is the distance between R (pivot) and S (end of the loudspeaker), d_r is the height of the pivot, d_m is the distance between the microphone and the road surface, and the angles β and θ refer to the leaning of the probe (loudspeaker-microphone system). Under these hypotheses the following equations refer to the geometry of the problem:

$$d_{RS} \cdot \cos\beta = d_{RS'} \qquad (13)$$

$$d_{RS} \cdot \sin\beta = d_{SS'} \qquad (14)$$

$$d_r - d_m - d_{RS'} = d_{S'T'} \quad (15)$$

$$x - d_{SS'} = d_{TM} = d_p \quad (16)$$

$$\tan \vartheta = \frac{d_p}{d_{S'T'} + 2 \cdot d_m} \quad (17)$$

$$\vartheta = \arctan \frac{d_p}{d_{S'T'} + 2 \cdot d_m} \quad (18)$$

$$d_{RM} \cdot \sin \beta = x \quad (19)$$

$$x = \sqrt{d_{RM}^2 - (d_r - d_m)^2} \quad (20)$$

$$d_{RM} \cdot \cos \beta = d_r - d_m \quad (21)$$

$$\tan \beta = \frac{x}{d_r - d_m} \quad (22)$$

$$\beta = \arctan \frac{x}{d_r - d_m} \quad (23)$$

Surface texture

ISO Standards 13473-1 and 13473-2 defines texture as: “the deviation of a pavement surface from a true planar surface”. Surface texture is usually supposed to be the superposition of "many" elementary components (harmonics). Four specific domains of texture can be defined: micro, macro, mega and roughness. Each one has a given range of amplitudes and wavelengths (x-axis) and affects tire-road interaction, see Figure 3 (Praticò *et al.* 2010).

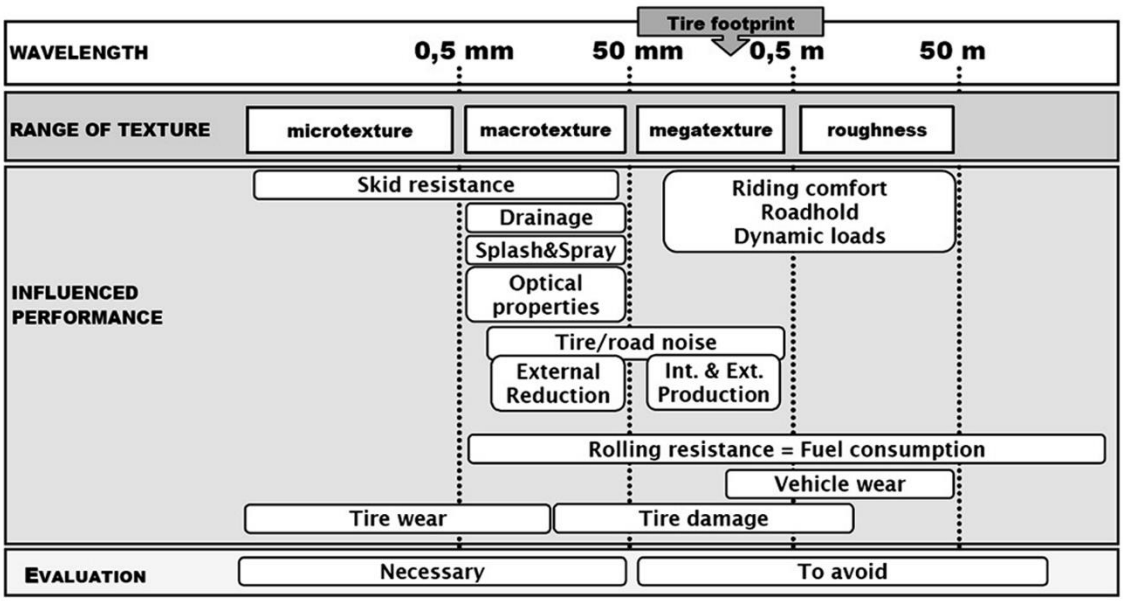

Figure 3 Texture and tyre–road interaction.

In studying road-tire interaction, two main classes of indicators can be used for the characterization of a pavement surface: *extrinsic* (or functional) and *intrinsic* (see Fig.4 and Tables A2-A4 in the annex) (Boscaino and Praticò 2001):

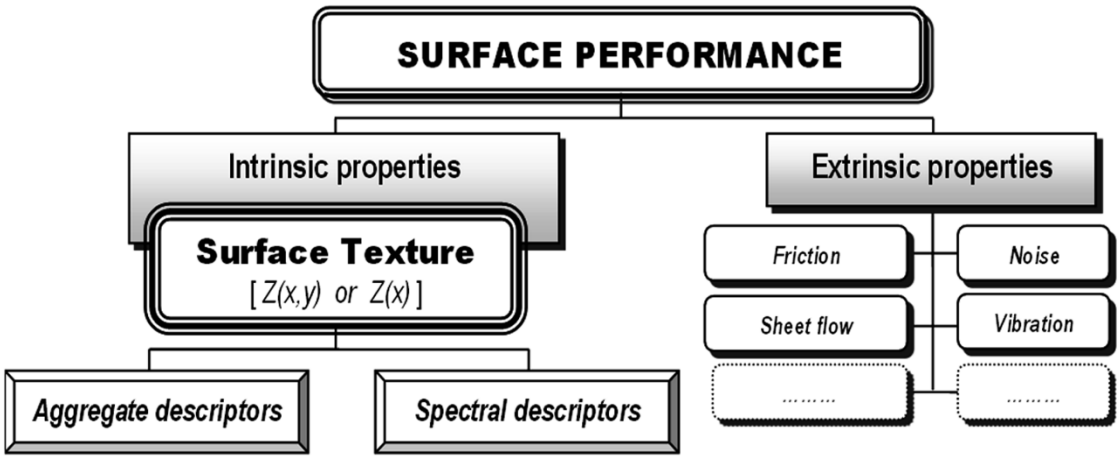

Figure 4 Road surface performance characterisation.

- *Extrinsic indicators refer to performance which are* strictly correlated with texture, such as outflow time, or friction (see Table A2).

- *Intrinsic indicators* are based on surveying and analysing surface geometry and interpreting it by appropriate algorithms and hypotheses;

Intrinsic criteria may be divided into two other subsets:

- *aggregate descriptors*, which are referred to all the surveyed wavelengths (see Table A3);
- space-frequency or *spectral descriptors*. These are obtained by imaging pavement profile as the superposition of "many" elementary components (harmonics), which are properly connected to a single wavelength in terms of Fourier analysis (see Table A4).

For the experimental application, among the intrinsic descriptors, the following were considered: MPDiso (ID = 14), ETDiso (ID = 45) and Lt (ID = 56). MPDiso and ETDiso provide aggregate information on macro-texture amplitudes, while Lt refers to the amplitudes of pavement texture for different wavelengths (see tables in Appendix).

Experiments

Table 1 summarizes the experimental plan, while Fig.5 illustrates the setup.

Geometrical configurations for acoustic absorption measurements (α)				
dr ***(cm)***	***dm*** ***(cm)***	***x*** ***(cm)***	***β*** ***(deg)***	***θ*** ***(deg)***
158.5	25.0	0.0	0	0
158.5	42.9	66.9	30	18
158.5	92.0	115.8	60	25
158.5	158.0	133.5	90	23
158.5	252.9	96.4	136	9
158.5	292.0	0.0	180	0
158.5	158.5	-133.5	-90	-23
158.5	92.0	-115.8	-60	-25

158.5		43.0	66.9		-30	-18	
158.5		25	0		0	0	
Surface texture indicators (MPDiso, ETDiso, Lt)							
	Profile 1	***Profile 2***	***Profile 3***	***Profile 4***	***Profile 5***	***Profile 6***	***Profile 7***
x (cm)	-300	-200	-100	0	100	200	300

Table 1 Experimental plan.

The height of the pivot (R, center of rotation of the probe, with respect to the road surface, see Fig.2) was held constant (d_r=1.585m) and the acoustical absorption coefficient (vector) was derived for different angles which in turn corresponds to different (x, d_m) couples, where x is the abscissa and d_m is the microphone height.

Seven parallel texture profiles were surveyed and analysed in the pertaining area, each one passing for a given x (-3.00, -2.00, -1.00, 0, 1.00, 2.00, 3.00 m), see Table 1 and Fig.2 (where the independent variable x is specified). From the above profiles, aggregate and spectral indicators were derived (see tables A2 and A3 in the annex).

Fig. 5 refers to the measurement setup system (acoustic absorption).

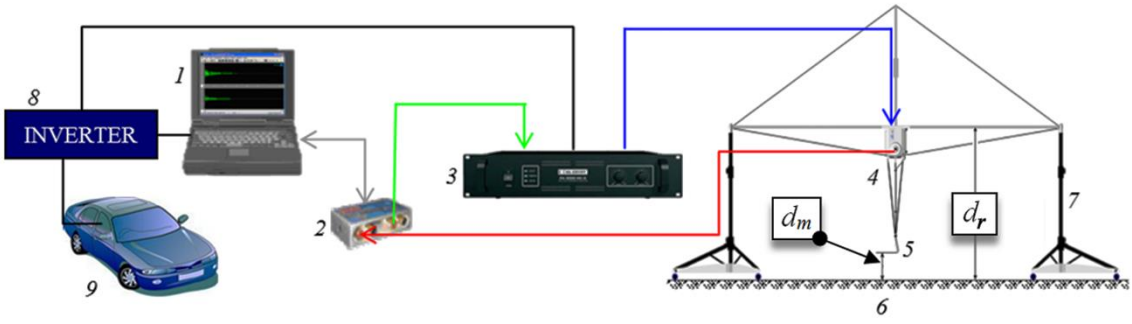

Figure 5 Measurement setup system.

Legend of figure 5:

1: Hardware and software system (signal generation and recording; data analysis); 2: USB/audio interface; 3: Amplifier; 4: Loudspeaker of the probe; 5: Microphone of the

probe; 6: Road surface; 7: Probe frame; 8: Inverter DC/AC; 9: Car (energy supply).

Note that the number of repetitions of measurements for each angle were 4·15 (four cycles; 15 measures *per* cycle; Impulse response, IR) and 4·5 (free-field measurement, FF). For each (15+5) data set, the averages underwent two successive procedures: subtraction (IR-FF) and time windowing (a five-seconds time window similar the so-called called Adrienne window was used).

Figures 6 to 12 show results. Figs 6 to 8 refer to acoustical measurements.

As mentioned before, the pavements under investigation were porous mixes (high air void content; thickness: 0.05 m), on impermeable binder courses (low air void content; thickness: 0.07 m). PEMs are rigid frame porous materials. Due to their particular pores, tortuosity and resistivity, these types of pavements present a maximum of the absorption coefficient of 0.6–0.9 for frequencies in the range 800–1200 Hz (Sandberg and Ejsmont 2002). As for the absorption coefficient, maximum point (Hz) and maximum value (dimensionless) depend mainly on resistivity, air void content and tortousity. Under the conditions of the experiments, variations of the above parameters can probably depend on the effective pores 'perceived' by the device and on the geometry of the problem (coupling between pavement and free field). Figure 6 summarises the main results (each plot a–e includes four absorption spectra, each one of which derived from 15 measures, and one average absorption spectrum). Figure 6(d) illustrates the dependence of standard deviation (y-axis) on frequencies (Hz, x-axis). The following observations were derived: (i) the highest absorption coefficient ranged from 0.83 to 0.98; (ii) the absolute optimum frequency (i.e. the first maximum point of the absorption coefficient, e.g. the frequency which corresponded to the highest absorption coefficient in the domain) ranged from 630 to 1000 Hz; (iii) another relative maximum of the absorption

curve might be located at frequencies higher than 4000 Hz; (iv) the average absorption coefficient in 125–4000 Hz ranged from 0.41 to 0.79; (v) the lowest absorption coefficient ranged from 0.20 to 0.55; (i) the standard deviation, for a given angle and a given frequency, ranged from 0.01 to 0.10, with an average of 0.03. These data were successfully compared with that in Roovers et al. (2004). The corresponding coefficient of variation (%) ranged from 1.6 to 17.0 (250 Hz), with an average of 6.9. Lower frequencies yielded higher standard deviations and higher coefficients of variation, while optimum frequencies yielded lower standard deviations and lower coefficients of variations.

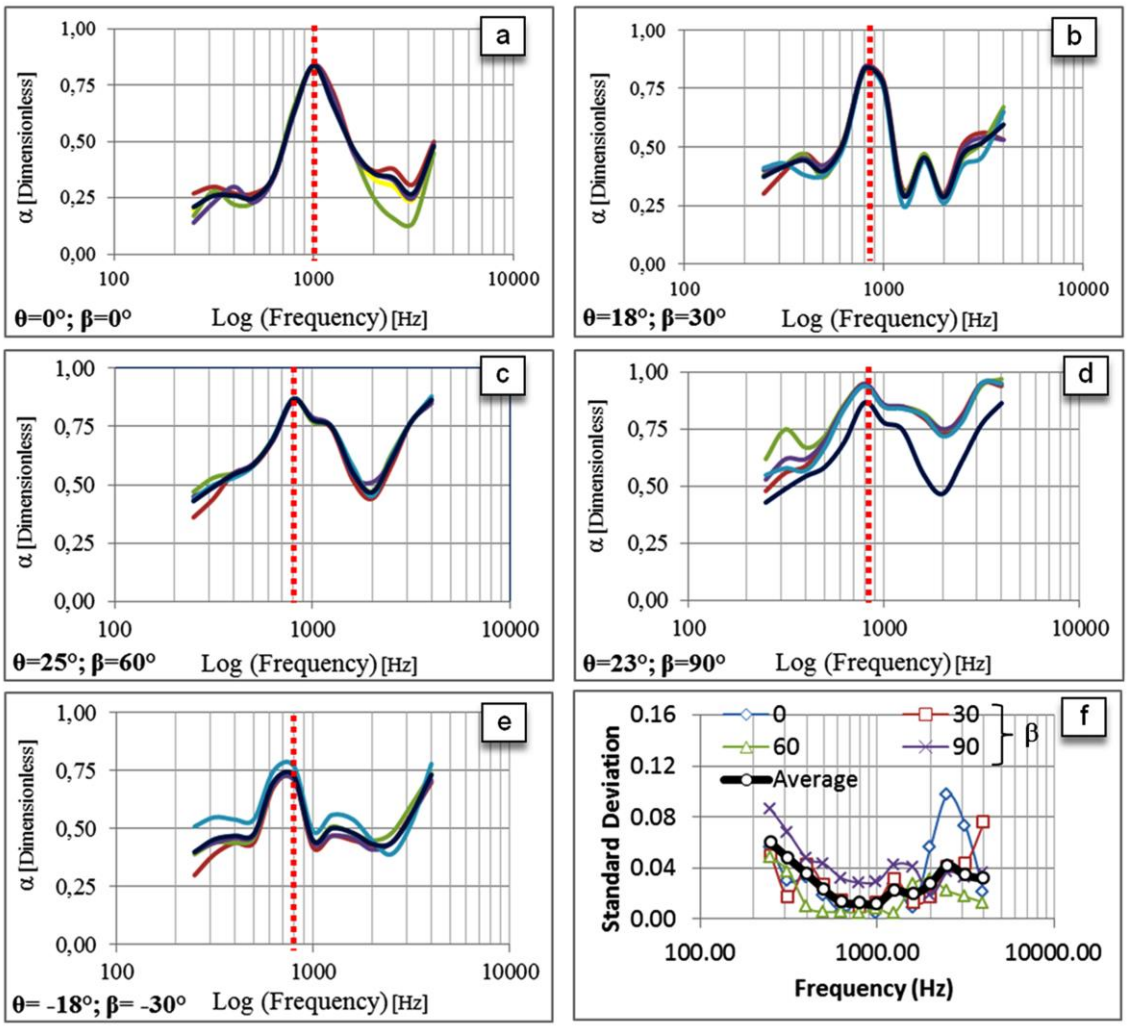

Figure 6 Sound absorption spectra of the tested surface (dr = 1.585 m).

Figures 7 and 8 refer to the highest absorption coefficient (in magnitude, Fig.7 and frequency, Fig.8).

The polar angular plot in fig. 7 (dotted line) refers to the absorption coefficient (highest value in the range 125-4000Hz), α, at some angle, between 0 and 360 degrees (polar coordinate system).

Each point on the plot is determined by a distance from the fixed point (pole, red circle at the centre) and an angle from a fixed direction. The ray from the pole in the fixed direction is the polar axis. The distance from the pole (radial coordinate or radius) is the absorption coefficient, and the angle (the angular coordinate or polar angle or azimuth) refers to the angle used in the measure of the absorption coefficient by the Adrienne method. The polar angle of the plot corresponds to β-90° (degs).

Note that the most common angle is -90 degrees (β=0, loudspeaker and microphone towards the pavement) but several European contract specifications (ANAS 2008) require an angle (which is supposed to be β=polar angle+90°) close to 30 degrees.

Note that in the same polar angular plot two reference curves are plotted (solid lines), which refer to 1 (upper limit) and 0.8 (reference value). The closer to 90° (free field, β=180°) the position of the device resulted, the closer to 1 α resulted (maximum theoretical absorption coefficient, corresponding to the free field condition). In contrast, the closer to the pavement (β=0°), the closer to 0.8 α resulted.

By referring to the three average absorption coefficients (mean value in 400-660Hz, mean value in 800-1250Hz, mean value in 1600/2500 Hz, as stated in quality assurance requirements - ANAS), the following new equation was derived:

$$\alpha_{f1,f2} = 1 - a_{f1,f2} \cdot \exp\left(\frac{-b \cdot \beta}{180 - \beta}\right) \quad (24)$$

where: i) $\alpha_{f1,f2}$ is the average absorption coefficient in the given frequency range (e.g., 400-630Hz), $a_{f1,f2}$ (dimensionless, positive) is a coefficient to calibrate based on the specific range of frequencies, b (dimensionless, positive) is a coefficient to calibrate (which can be considered common to the above three ranges), β is the rotation angle of the probe (degrees, °, range of variation in the algorithm: 0→180). Note that, under the above hypotheses, $\alpha_{f1,f2}$ is defined in (0, 1).

Range of frequency (Hz)	$a_{f1,f2}$	b
400-630	0.73	1.50
800-1250	0.36	1.50
1600-2500	0.72	1.50

Table 2 Parameters for the expression of the average absorption coefficient as a function of the angle.

Note that, due to contract specifications, the difference between $\alpha_{f1,f2}$ at 30° and $\alpha_{f1,f2}$ at 0° is a crucial factor in terms of quality control, quality assurance and contract administration. To this end, it is important to observe that equation (24) yields a difference of absorption coefficient (between $\alpha_{f1,f2}$ at 30° and $\alpha_{f1,f2}$ at 0°) which depends only on $a_{f1,f2}$ and b. Indeed, for the case study, this difference is given by $(1-a_{f1,f2})\cdot 0.26$ (see equation 24 and table 2). It follows that the increase in absorption coefficient (due to the absence of orthogonality) can be estimated as the 26% of the complement to 1 of the absorption coefficient. For example, if the average absorption coefficient in 400-630 Hz is 0.27, the increase will be the 26% of 0.73, which is 0.1.

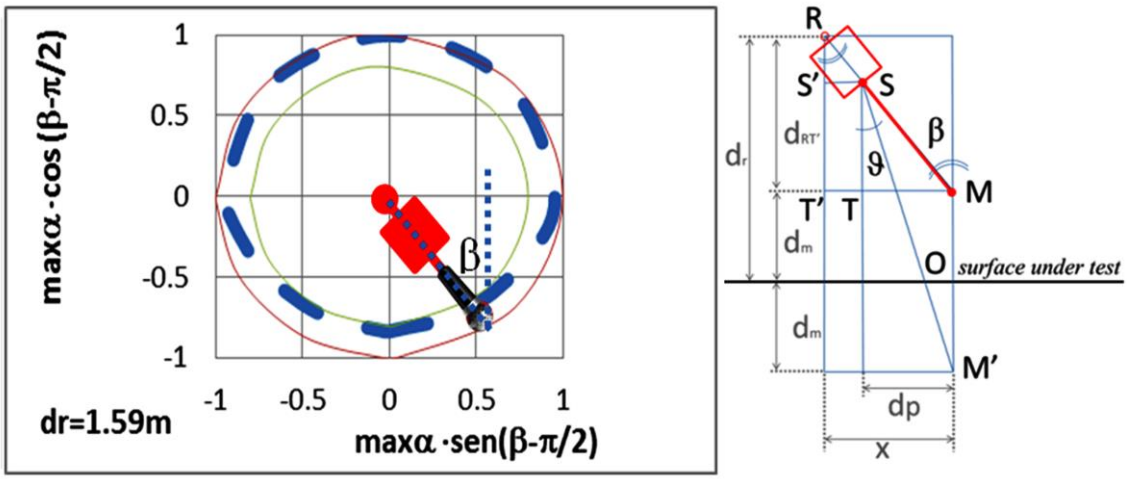

Figure 7 Maximum absorption coefficient vs. device angle (dr constant; polar angle of the plot = β − 90°).

By referring to the variations of the absorption spectrum, note that, from the data, it is possible to observe that the optimum frequency moves from 1000Hz to 800Hz (in the transition from β=0° to β=30°, see Fig. 8). Further experiments and analyses are needed on this topic to gain a better understanding of the real reasons of possible frequency shifts and their impact on loudness.

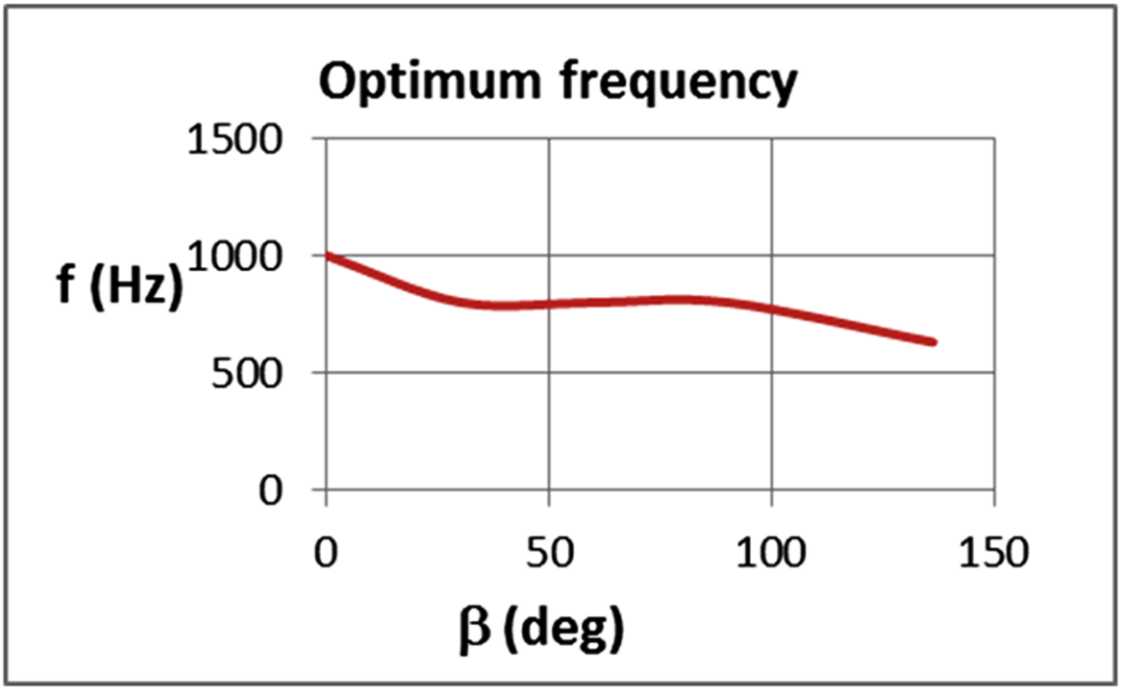

Figure 8 Optimum frequency versus angle.

Figures 9 to 12 and table 3 summarize texture investigations.

As is well known, road surface texture (wavelengths from 0.5mm to 500mm) affects tire-pavement noise and (together with air void content) the acoustic absorption coefficient (Boscaino and Praticò 2001). As a consequence, differences in surface texture could be strongly related to the results above illustrated. In order to reject or confirm this hypothesis and gather other information about the properties of the surface under investigation, seven profiles were surveyed.

The evaluation length was 1.5 m, in order to enable a one-thirdoctave- band λ_{max} (longest wavelength) of approximately 0.1 m, which is sufficient to cover the macrotexture range ($0.5 \cdot 10^{-3}$m-0.05m).

The following algorithms were applied to the profile in the aim of deriving the texture level (ISO 13473-4: 2008): i) interpolation of drop-outs; ii) offset and slope suppression; iii) windowing (A Hanning window and the profile $Z_{i,win}$ was obtained); iv)

Fast Fourier Transform.

The Fast Fourier Transform algorithm was applied to $Z_{i,win}$ as follows:

$$FFT = \sum_{i=0}^{N-1} Z_{i,win} \cdot e^{-j\cdot\left(\frac{2\pi k}{N}\right)i} \tag{25}$$

Finally the texture level was obtained as follows:

$$L_{txk} = 10 \cdot Log_{10}\left(2 \cdot \left|\frac{FFT}{N}\right|^2\right) \tag{26}$$

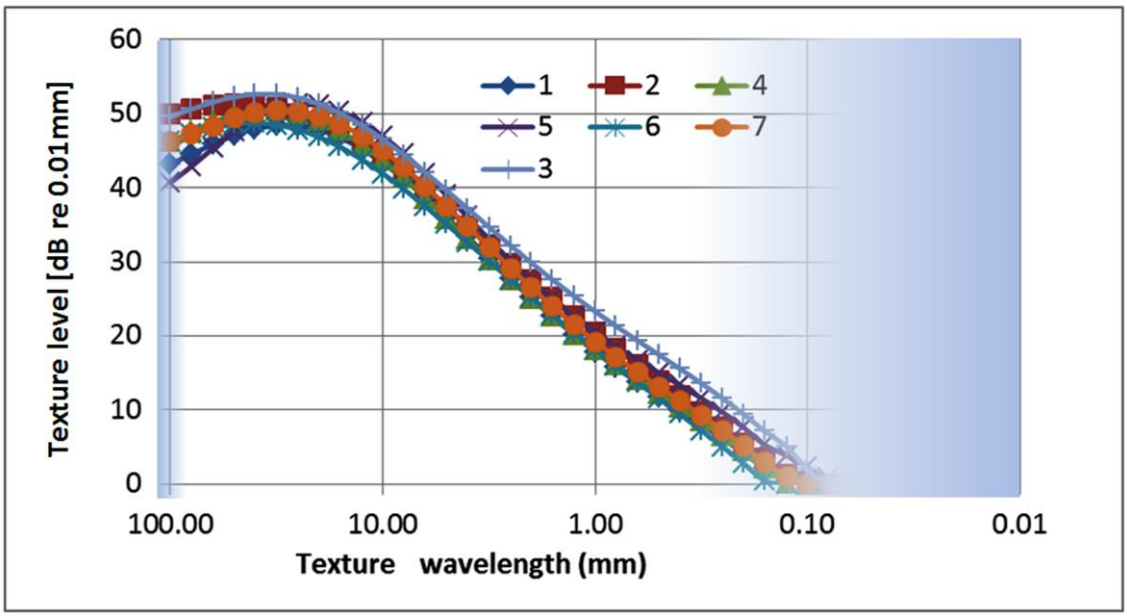

Figure 9 Texture spectra (see Table A4).

Figures 9 and 10 refer to texture spectra. Y-axis reports the texture level, while x-axis refers to texture wavelengths. The highest value ranged from 48.4 dB (profile 1) to 52.6 dB (profile 3). Within the domain of the macrotexture, the level ranged from 11.6 dB to 52.6 dB, with an average of 35.3 dB. These values were successfully compared with the

literature (Boscaino and Praticò 2001; Goubert and Bergiers 2012).

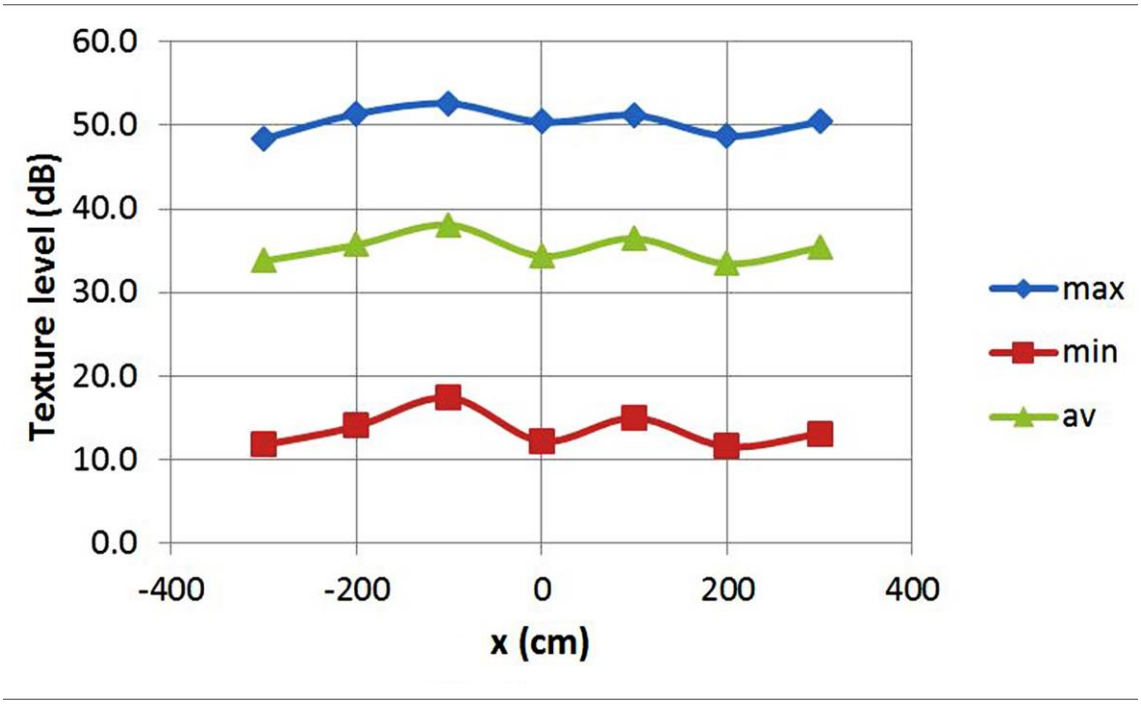

Figure 10 Minimum (min), maximum (max) and average (av) value of texture spectrum.

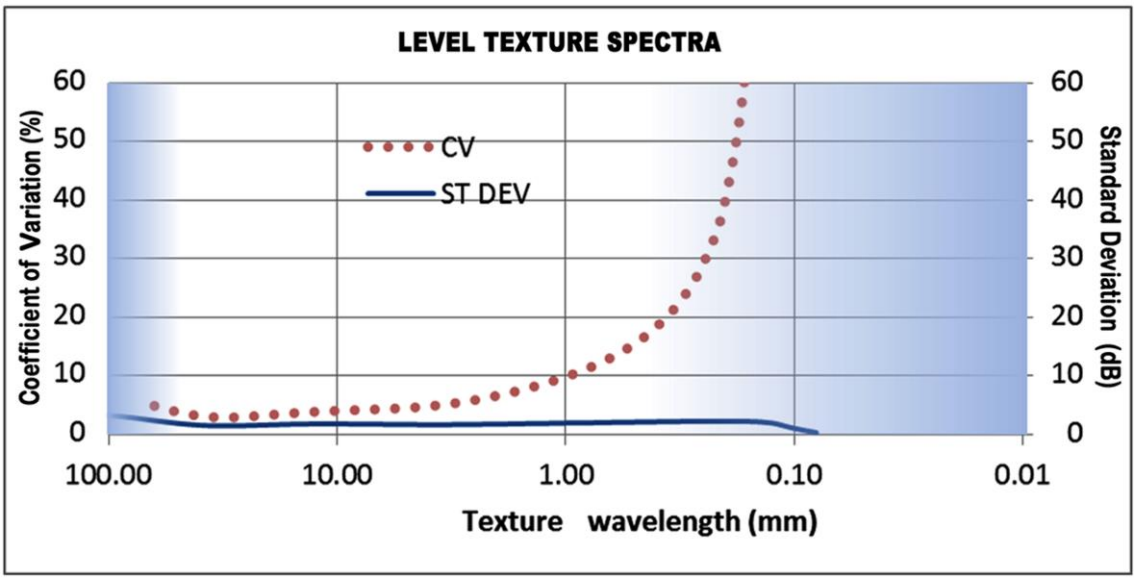

Figure 11 Standard deviation and coefficient of variation of texture spectra.

By referring to the texture spectra, Fig. 11 illustrates the standard deviation and the coefficient of variation (CV, standard deviation-to-average ratio, in percentage) as a function of the wavelength. In the macrotexture range, the standard deviation ranged from 1.4 dB to 2.1 dB (average: 1.8 dB), while the CV ranged from 2.9 to 15.5, with an average of 6.1. It is noted that the standard deviation exhibited a quite constant value, and, due to the appreciable variation of texture spectra, the coefficient of variation presented a considerable increase in the boundary between macro and microtexture. This fact might depend on the accuracy of the device and/or on the variable state of the surface of the grains (spoiled vs. unspoiled). Furthermore, note that the average coefficient of variation was similar to the one obtained for the acoustical absorption coefficient.

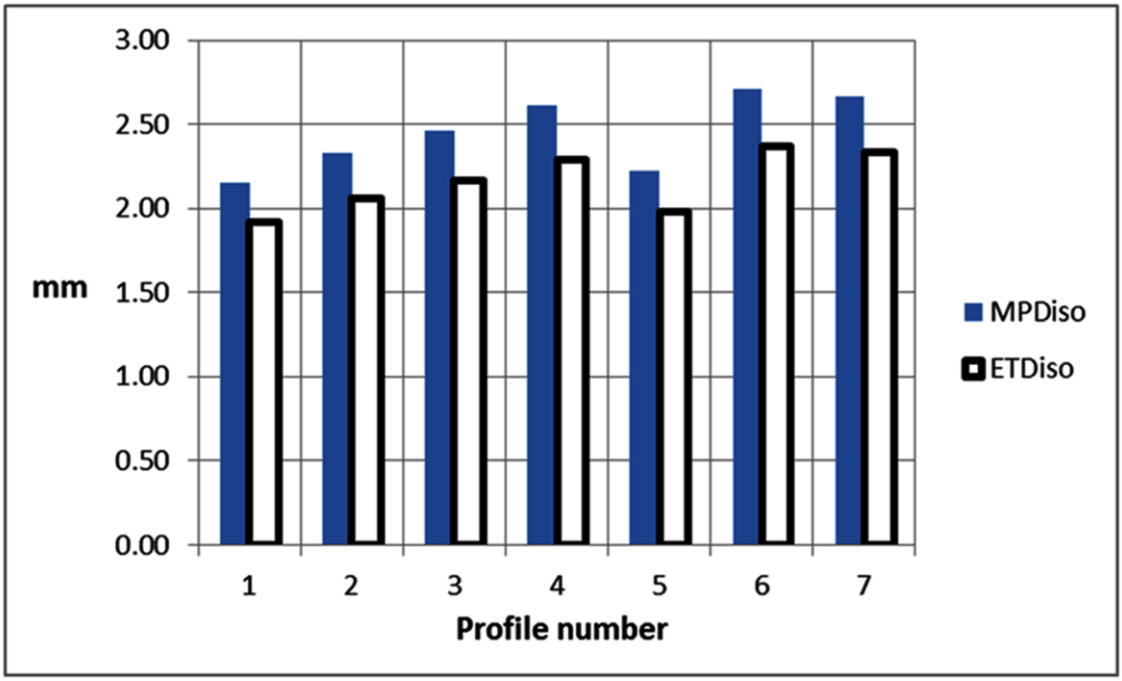

Figure 12 MPDiso and ETDiso.

Figure 12 and table 3 illustrate how the aggregate indicators (MPDiso and ETDiso) varied for the considered profiles. Standard deviation was around 0.2 mm with a

coefficient of variation in the range 8-9, not very dissimilar from the ones obtained for the texture level and the acoustic absorption.

	MPD_{ISO}	ETD_{ISO}
Standard dev.	0.22	0.18
CV (%)	9.07	8.23

Table 3 Standard deviation and coefficient of variation of texture aggregate indicators.

Based on the above results, the following tentative theoretical framework can be set out: i) the absorption coefficient depends on incidence angle according to the set of equations described in the standards ISO 13472-1; ii) in the transition from the orthogonal position (pavement) to the opposite (free field), the absorption coefficient increases monotonically from a minimum condition (full pavement contribution) to a maximum condition (null pavement contribution); iii) the increasing and monotonic behaviour affects all the frequencies.

Conclusions

A dependence of the absorption coefficient on the angle was found. A non-normal position of the device is likely to imply an average increase of the acoustical absorption in the three frequency ranges usually considered (400–630 Hz, 800–1250 Hz, 1600–2500 Hz).

The synergetic assessment of surface texture indicators permitted to derive that the dependence on angles is not affected by texture-related issues or systematic variations.

Indeed the surface texture did not present any corresponding systematic variability.

For a constant dr (fixed height of the pivot), the absorption coefficient at 30 degrees (beta) resulted on average 1.4 times the absorption coefficient at 0 degrees (beta). This fact is due to the paths of the reflected acoustic waves, the remaining factors remaining statistically constant.

Standard deviations were on average 0.03 for the acoustical absorption coefficient, 0.2 for the texture aggregate indicators and 1.8 for the texture level. Despite this, coefficients of variation for the three considered classes of surface indicators ranged in a narrow range (6–9).

The setup of the device for non-normal measurements needed optimisation due to the difficulty in estimating the angle. It is recommended that a system for fixing and adjusting the device to a certain angle is conceived and provided. Future research will address a number of these challenges, using a systems approach to better understand how acoustic absorption and surface texture influence one another within a whole.

Appendix

Table A1. Main symbols

Variable	Definition	Unit of measure
*	symbol of convolution	-
c	speed of sound in air (m/s)	m/s
d(S,O)	loudspeaker-surface under test distance	Meters
d(S,O,M)	loudspeaker-surface under test- microphone distance	Meters
d_m	Height above the test surface of the microphone - microphone altitude	Meters
Dp	projection of the loudspeaker -microphone distance	Meters
Dr	pivot altitude	Meters
d_{RM}	=1.335 m, length of Zircon probe	Meters
d_{RS}	= 0.335 m, is the height of the Zircon probe box	Meters

$d_{RS'}$	vertical projection of dRS	Meters
d_s	Height above the test surface of the loudspeaker -loudspeaker altitude	Meters
$d_{S'T'}$	vertical projection of dSM	Meters
d_{SM}	= 1 m, is the loudspeaker-microphone distance	Meters
$d_{SS'}$	horizontal projection of dRS	Meters
d_{TM}	horizontal projection of dSM	Meters
f_{co}	filter cut-off frequency	Hertz
f_s	sample rate	Hertz
$H_i(f)$	Transfer function of the direct path impulse response, i.e. spectrum of the sound pressure wave travelling from the sound source to the surface under test, as detected by the microphone	"
$h_i(t)$	direct component of the impulse response of the road surface tested	,,
$H_{i,\theta}(f)$	Transfer function of the direct path impulse response, i.e. spectrum of the sound pressure wave travelling from the sound source to the surface under test, as detected by the microphone relating to the measure to not normal incidence	"
$h_m(n\Delta t)$	overall microphone response of the surface under investigation	**Dimensionless**
$h_{m,pre}(n\Delta t)$	microphone actual response (which includes secondary, undesirable effects)	"
$h_n(n\Delta t)$	response sampled by the microphone that relative to the background noise	"
$h_n(t)$	component of the impulse response relative to the background noise	,,
$h_r(t)$	reflected component of the impulse response of the road surface tested	,,
$H_r(f)$	Transfer function of the reflected path impulse response, i.e., spectrum of the sound pressure wave reflected by the surface under test, as detected by the microphone	"
$H_{r,\theta}(f)$	Transfer function of the reflected path impulse response, i.e., spectrum of the sound pressure wave reflected by the surface under test, as detected by the microphone relating to the measure to not normal incidence	"
J	subscripted which indicates the *parasitic reflections*	-
K_r	geometrical spreading factor	Dimensionless
Kr, θ	geometrical spreading factor relating to the measure to not normal incidence	Dimensionless
$K_{r,j}$	geometrical spreading factor for parasitic reflections	"
L	length of the binary sequence (of the signal)	Dimensionless
M	microphone of the probe Ziron	-
N	order of the MLS	Dimensionless
$Q_p(f)$	sound pressure reflection factor of the surface under test	"
$Q_{p,ref,meas}(f)$	sound pressure reflection factor of the reference surface under test measured in-situ	"
$Q_{p,road}(f)$	sound pressure reflection factor of the road surface under test	"
$Q_{p,road,meas}(f)$	sound pressure reflection factor of the road surface under test measured in-situ	"
$Q_W(f)$	sound power reflection factor of the surface under test	"

$Q_{W,\,road,\,ref}$ (f)	sound power reflection factor of the reference surface	“
$Q_{W,\,road,meas}$ (f)	sound power reflection factor of the road surface under test measured in-situ	“
R	effective radius of the circular surface which is interested by the reflection	Meters
R	center of rotation of the probe (pivot)	-
$r_p(t)$	reflection factor of the surface under test	“
$r_{p,j}$ (t)	reflection factor of an object that does not belong to the surface under test	“
S	loudspeaker of the probe Ziron	-
s(nΔt)	pseudorandom MLS (Maximum-Length Sequence) signal	“
s(-nΔt)	pseudorandom MLS signal reversed in the time domain	“
T_s	time length of one cycle of an MLS signal	Seconds
T_w	duration of the time window applied to the impulse response	Milliseconds
X	Horizontal projection of the pivot-to-microphone distance	Meters
$\alpha_{\theta}(f)$	Sound absorption coefficient obtained by measurements at not normal incidence	Dimensionless
α(f)	Sound absorption coefficient	“
B	rotation angle of the probe;	Degrees
Δt	sampling time (the reciprocal of the sample rate)	Seconds
Θ	angle of incidence of the sound field	Degrees
$\Phi_{s,m}(n\Delta t)$	result of the circular correlation between s(-nΔt) and $h_{m,pre}$ (nΔt)	Dimensionless
τ	air temperature measured in situ	Centigrade degree

Table A2. Extrinsic descriptors

N°	***ID***	***Unit***	***Description***
61	a, a_0	$[L^0]$	a: sound absorption coefficient (→ noise nuisance); a_0: sound absorption coefficient in normal incidence (→ noise nuisance).
62	BPN	$[L^0]$	British Portable Tester Number (BPN, → pendulum friction measurement)
63	SFC [CAT]	$[L^0]$	Sideway force coefficient - SFC (measured, for example, by SCRIM)
64	GN	$[L^0]$	Grip number (GN device = Grip Tester)
65	Drainability	$[L^3/T]$	Drainability
66	IRI	$[L^0]$	International Roughness Index (→ Comfort)
67	RCI	$[L^0]$	Riding Comfort Index (→ Comfort)
68	IFI	$[L^0]$	International Friction Index

Table A3. Aggregate intrinsic indicators

N°	*ID*	*Unit*	*Description*
01	n/L	$[L^{-1}]$	Average asperity density
02	R_{max}	[L]	Maximum peak-to-valley height
03	R_t	[L]	Peak-to-valley height
04	R_z	[L]	Average peak-to-valley height
05	MAA,(Σh/n)	[L]	Mean Apparent Amplitude
06	(Σh/n)	[L]	Average Asperity height
07	(Σh/n)/(L/n)	[L°]	Average shape factor
08	$\bar{Z}$	[L]	$z_{media}=\Sigma_i z_i p(z_i)$. Mean line, arithmetic mean
09	R_a	[L]	$R_a=\Sigma_i \mid z_i - z_{media} \mid \cdot p(z_i)$. Average Roughness or Centre-line average
10	R_u	[L]	z_{max}-z_{media}. Levelling Depth,
11	R_m	[L]	Mean Depth. The RMD Rut Mean Depth as defined in E1703-E1703M-95 ASTM can be related to this parameter.
12	R_p	[L]	$R_p=\Sigma_i(z_{max}-z_i)\cdot p(z_i)$. Depth of surface roughness
13 14	PD; MPDiso MPD Short	[L]	Profile Depth; Mean Profile Depth measured for wavelengths between 2.5 and 100 mm, according to the Standard ISO 13473-1. The parameter MPD Short (measured, for example, with a Texture Meter mounted on a SCRIM) is measured for wavelengths of between 2.5 and 10 mm.
15	z_4	$[L^0]$	$z_4=[\Sigma(\Delta x_i)_+ - \Sigma(\Delta x_i)_-]/L$. Parameter involving the number of profile segments with a positive difference in elevation
16 17 18 19 & 20	R_q, σ; z_1; SD; SMTD; CSMTD	[L]	$R_q \approx \sigma \approx z_1 \approx [\Sigma(z-z_{media})^2 p(z)]^{0.5}$. Root-mean-square roughness; Standard Root-mean-square Standard Deviation; Sensor Measured Texture Depth; Corrected SMTD;
21	TDMA	[L]	$\rightarrow \sigma$. Texture depth of macrotexture
22	S_k	$[L^0]$	$S_k=\sigma^{-3}\cdot\Sigma(z-z_{media})^3\cdot p(z)$. Skewness
23	K	[L]	$S_k=\sigma^{-4}\cdot\Sigma(z-z_{media})^4\cdot p(z)$. Kurtosis
24	z_2	$[L^0]$	$z_2=[\Sigma z'^2 p(z)]^{0.5}$. RMS difference in elevation
25	z_3	$[L^{-1}]$	$z_3=[\Sigma z''^2 \cdot p(z)]^{0.5}$. RMS value of second derivative
26	r_e	[L]	$r_e=r*N_k$. Effective radius
27	D_f	$[L^0]$	$\rightarrow$ $l=k*u^{1-Df}$. Fractal dimension D_f
28	W	[L]	Mean groove width
29	D	[L]	Mean groove depth
30	S	[L]	Span (pitch)
31	VarW	$[L^2]$	Variance in width W
32	VarD	$[L^2]$	Variance in depth D
33	VarS	$[L^2]$	Variance in span
34	NumGRV	$[L^0]$	Number of grooves
35	NumGRV $_{D\leq(xi)}$	$[L^0]$	Number of grooves with depth D less than or equal to x_i''; x_i is generally in inches
36	NumGRV $_{W\leq(1/8)}$	$[L^0]$	Number of grooves in the section of profile with width W less than or equal to 1/8'' (3.175 mm)
37	NumGRV$_{G\leq(1/8)}$	$[L^0]$	Number of grooves with width W or Depth D less than or equal to 1/8''
38	TAWRG	$[L^0]$	Total area within the 10 foot segments with recognizable grooves
39 40	MPDwG MPDnoG	[L]	Mean profile depth (MPD) with grooves; Mean profile depth (MPD) with no grooves
41	A_r	[L]	$A_r=n^{-1}\cdot(\Sigma a_{ri})$. Roughness width (Mean distance between the peaks n in the profile)
42	A_w	[L]	$A_w=n^{-1}\cdot(\Sigma a_{wi})$. Mean waviness width (Mean distance between the peaks n in the profile)
43	l_t (c)	[L]	$l_t(c)=\Sigma l_i(c)$. Bearing length at height c from mean line
44	λ_a	[L]	$\lambda=2\pi R_a$/(mean slope). Average wavelength
45 46 47	MTD ≈ ETD HS NASA G.S.P.	[L]	Mean Texture Depth; Hauteur de sable; NASA Grease Smear Parameter. These are two-variable intrinsic indicators experimental analysis of which can provide an estimate of the ratio between $\int_S z(x,y)\,dx\,dy$ and $\int_S dx\,dy$, a first order moment I. For maintenance, the MTD can be estimated by the formula ETDiso=0,2 mm+0,8MPD (ETD=Estimated Texture Depth, according to Standard ISO 13473-1). Many other acronyms designate indicators measured with different devices (often high-speed) which are similar to the parameter HS.
48 - 53	A, B, C, D, E, F		Qualitative and quantitative parameters related macrotexture and microtexture, defined in ASTM E770

Table A4. Spectral intrinsic indicators

N°	*ID*	*Unit*	*Description*
54	PSD	$[L^3]$	Power Spectral Density
55	PS	$[L^2]$	Power Spectrum
56	ck , L_T	$[L^0]$	Texture amplitudes (ck), Texture Level (LT)
57	a_5, a_{mega}	[L]	Texture amplitude for the wavelength of 5mm (a_5, established with reference to the band centres of 4mm, 5mm and 6.3mm) or 25mm (a_{mega}, based on the amplitudes for 20mm, 25mm and 31mm)
58	H_{APL};	[L]	Amplitude of the irregularities for a zone with a specified wavelength
59	INBO;	$[L^0]$	Class of indicators that are determined by associated a scalar quantity of between 0 and 10 to short, medium and long waves (INBO, Notation par Bandes d'Onde - NBO –Wave Band Rating).
60	ENDt	$[L^0]$	Single number rating. It expresses the expected pass-by Noise level Difference (dB(A), 80km/h, passenger car tyres) caused from a texture level variation of the road surface. This descriptor is estimated from the texture Level (L_T , ID=n°56) that is an intrinsic spectral descriptor. The ENDt is calculated according to the Standards ISO 13473-1, ISO 13473-3, ISO/CD TS 13473-4 and ISO 10844:2011 (see also SILVIA project reports).

References

1. AASHTO TP76: 2009, Standard method of test for measurement of tire/pavement noise using the on-board sound intensity (OBSI) method. [Google Scholar]
2. Alvarez, A.E., Martin, A.E., and Estakhri, C., 2010. Internal structure of compacted permeable friction course mixtures. Construction and Building Materials, 24 (6), 1027–1035. [Crossref], [Web of Science ®], [Google Scholar]
3. Alvarez de Sotomayor, R., et al., 2012. Measurement of sound absorption coefficient of road surfaces in situ. In: 7th symposium on pavement surface characteristics, 18–21 September 2012 Norfolk Waterside US. [Google Scholar]
4. ANAS, 2008. Gestione Delle Pavimentazioni Stradali - Linee Guida di Progetto e Norme Tecniche Prestazionali [Pavement management – design basics and performance-based standards]. [Google Scholar]
5. Attenborough, K., 1983. Acoustical characteristics of rigid fibrous absorbents and granular materials. Journal of the Acoustical Society of America, 73, 785–799. [Crossref], [Web of Science ®], [Google Scholar]
6. Biligiri, K.P., 2013. Effect of pavement materials' damping properties on tyre/road noise characteristics. Construction and Building Materials, 49, 223–232. [Crossref], [Web of Science ®], [Google Scholar]
7. Boscaino, G., Celauro, B., Celauro, C., and Amadore, A., 2009. Evaluation of the laboratory prediction of surface properties of bituminous mixtures. Construction and Building Materials, 23 (2), 943–952. [Crossref], [Web of Science ®], [Google Scholar]
8. Boscaino, G. and Praticò, F.G., 2001. Classification et inventaire des indicateurs de la texture superficielle des revêtements des chaussées. Bullettin des Laboratoires des PontsetChaussées, 234, 17–34. [Google Scholar]

9. Boscaino, G., Praticò, F.G., and Vaiana, R., 2005. Tyre/road noise on different road pavements: synergetic influence of acoustical absorbing coefficient and surface texture. In: Proceedings of 10th EAEC European congress, JUMV (Yugoslav Society of Automotive Engineers), 30th May–1st June 2005 Belgrade. [Google Scholar]
10. European Commission, 1998. Test methods for the acoustic performance of road traffic noise reducing devices SMT project MAT1-CT94049 'Adrienne'. Final report 1-95/12-97. [Google Scholar]
11. European Commission, 2002. Directive on environmental noise, 2002/49/CE. 25th June 2002, DOCE L 89, 7/18/02. [Google Scholar]
12. Filianoti, P., 2001. Return periods of summer-time sea storms in the central Mediterranean sea. Environmental studies. In: Coastal engineering V, transaction: the built environment. Vol. 58. Southampton: WIT Press, 299–308. [Google Scholar]
13. Freitas, E., et al., 2012. Traffic noise abatement: how different pavements, vehicle speeds and traffic densities affect annoyance levels. Transportation Research Part D, 17 (4), 321–326. [Crossref], [Web of Science ®], [Google Scholar]
14. Frías, M., et al., 2011. Development of blended cement mortars with acoustic properties using petroleum coke. Construction and Building Materials, 25 (2), 1086–1092. [Crossref], [Web of Science ®], [Google Scholar]
15. Goubert, L. and Bergiers, A., 2012. About the reproducibility of road texture profiles in the macro-mega range and the problem of spikes. In: 7th symposium on pavement surface characteristics, 18–21 September 2012 Norfolk Waterside US. [Google Scholar]
16. Guidorzi, P. and Garai, M., 2008. Signal analysis in the sound absorption measurement procedure: the importance of time subtraction and reference surface corrections. In: Proceedings of acoustics '08 Paris, 29 June–4 July 2008 Paris, 1755–1760. [Google Scholar]
17. ISO 10534-1:1996, Acoustics: determination of sound absorption coefficient and impedance in impedance tubes – Part 1: method using standing wave ratio. [Google Scholar]
18. ISO 10534-2:1998, Acoustics: determination of sound absorption coefficient and impedance in impedance tubes – Part 2: transfer-function method. [Google Scholar]
19. ISO 10844:2011, Acoustics: specification of test tracks for measuring noise emitted by road vehicles and their tyres. [Google Scholar]
20. ISO 13472-1:2002, Acoustics: measurement of sound absorption properties of road surfaces in situ – part 1: extended surface method. [Google Scholar]
21. ISO 13472-2:2010, Acoustics: measurement of sound absorption properties of road surfaces in situ – Part 2: spot method for reflective surfaces. [Google Scholar]
22. ISO 13473-1: 1997, Characterization of pavement texture by use of surface profiles. Part 1: determination of mean profile depth. [Google Scholar]
23. ISO 13473-2: 2002, Characterization of pavement texture by use of surface profiles. Part 2: terminology related to pavement texture profile analysis. [Google Scholar]
24. ISO 13473-3: 2002, Characterization of pavement texture by use of surface profiles. Part 3: specifications and classification of profilometers. [Google Scholar]

25. ISO/CD TS 13473-4:2008, Characterization of pavement texture by use of surface profiles. Part 4: spectral analysis of texture profiles. [Google Scholar]
26. ISO/DIS 11819-2: 2002, Acoustics: method for measuring the influence of road surfaces on traffic noise – part 2: close-proximity (CPX) method. [Google Scholar]
27. Jimenez-Espadafor, F.J., et al., 2011. Optimal design of acoustic material from tire fluff. Materials and Design, 32 (6), 3608–3616. [Crossref], [Web of Science ®], [Google Scholar]
28. Kringos, N. and Scarpas, A., 2008. Physical and mechanical moisture susceptibility of asphaltic mixtures. International Journal of Solids and Structures, 45 (9), 2671–2685. [Crossref], [Web of Science ®], [Google Scholar]
29. Licitra, G., Teti, L., and Cerchiai, M., 2013. A modified close proximity method to evaluate the time trends of road pavements acoustical performances. Applied Acoustics, 76 (2014), 169–179. [Google Scholar]
30. Lin, W.-C. and Wang, W.-H., 2013. Measurement of sound absorption properties and traffic noise attenuation prediction of road pavement. In: Proceeding of 20th international congress on sound and vibration (ICSV20), 7–11 July 2013 Bangkok, Thailand. [Google Scholar]
31. Londhe, N., Rao, M.D., and Blough, J.R., 2009. Application of the ISO 13472-1 in situ technique for measuring the acoustic absorption coefficient of grass and artificial turf surfaces. Applied Acoustics, 70 (1), 129–141. [Crossref], [Web of Science ®], [Google Scholar]
32. Loprencipe, G. and Cantisani, G., 2013. Unified analysis of road pavement profiles for evaluation of surface characteristics. Modern Applied Science, 7 (8), 1–14. [Crossref], [Google Scholar]
33. Meegoda, J.N., et al., 2002. Correlation of surface texture, segregation and measurement of air voids. Washington, DC: Federal Highway Administration, U.S. Department of Transportation. FHWA-NJ-2002-026. [Google Scholar]
34. Mommertz, E., 1995. Angle-dependent in situ measurements of reflection coefficients using substraction technique. Applied Acoustics, 46 (3), 251–264. [Crossref], [Web of Science ®], [Google Scholar]
35. Morgan, P.A. and Watts, G.R., 2003. A novel approach to the acoustic characterisation of porous road surfaces. Applied Acoustics, 74 (12), 1171–1186. [Crossref], [Web of Science ®], [Google Scholar]
36. Praticò, F.G., 2001. Roads and loudness: a more comprehensive approach. Journal of Road Materials and Pavement Design, 2 (4), 359–377. [Taylor & Francis Online], [Google Scholar]
37. Praticò, F.G. and Anfosso-Lédée, F., 2012. Trends and issues in mitigating traffic noise through quiet pavements. Procedia: Social & Behavioral Sciences, 53, 203–212. [Crossref], [Google Scholar]
38. Praticò, F.G. and Vaiana, R., 2012. Improving infrastructure sustainability in suburban and urban areas: is porous asphalt the right answer? And how? In: Urban transport 2012. WIT transactions on the built environment. Vol. 128. Southampton: WIT Press, 673–684. [Crossref], [Google Scholar]
39. Praticò, F.G. and Vaiana, R., 2013. A study on volumetric versus surface properties of wearing courses. Construction and building materials, 38 (1), 766–775. [Crossref], [Web of Science ®], [Google Scholar]
40. Praticò, F.G., Vaiana, R., and Giunta, M., 2011. Recycling PEMs back to innovative, silent, permeable road surfaces. Vol. 5. In: 8th international

conference ‘environmental engineering’ May 19–20 May 2011. Vilnius, Lithuania, 1186–1192. [Google Scholar]
41. Praticò, F.G., Vaiana, R., and Giunta, M., 2012b. Sustainable rehabilitation of porous european mixes. In: ICSDC 2011, integrating sustainability practices in the construction industry, proceedings of the international conference on sustainable design and construction, 23–25 March 2011. Kansas City, USA, 535–541. [Crossref], [Google Scholar]
42. Praticò, F.G., et al., 2012a. Permeable wearing courses by recycling PEMs: strategies and technical procedures. Procedia: Social & Behavioral Sciences, 53, 276–285. [Crossref], [Google Scholar]
43. Praticò, F.G., et al., 2010. HMA composition versus surface characteristics: issues and perspectives to optimise road asset management. In: Proceedings of 2nd international conference on transport infrastructures, 4–6 August 2010. São Paulo, Brazil. Guimarães: Universidade do Minho – Escola de Engenharia, 549–561. [Google Scholar]
44. Roovers Mioduszewski, P., Van Blokland, G.J., and Ejsmond, J., 2004. The SilVia round-robin test on measurement devices for road surface acoustics. In: Proceedings of internoise 2004, August 2004 Prague, Czech Republic. [Google Scholar]
45. Sandberg, U. and Ejsmont, J.A., 2002. Tyre/road noise reference book. Kisa: INFORMEX, Harg. [Google Scholar]
46. Shen, W., et al., 2013. Investigation on polymer–rubber aggregate modified porous concrete. Construction and Building Materials, 38 (1), 667–674. [Crossref], [Web of Science ®], [Google Scholar]
47. UNI EN ISO 11819-1: 2004, Acustica - Misurazione dell'influenza delle superfici stradali sul rumore da traffico – Metodo statistico applicato al traffico passante [Acoustics – measurement of the influence of road surfaces on traffic noise – statistical pass-by method]. [Google Scholar]
48. UNI ISO 13472-1, 2004, Misurazione in situ del coefficiente di assorbimento acustico di superfici stradali – Metodo della superficie estesa [Acoustics – measurement of sound absorption properties of road surfaces in situ – extended surface method]. [Google Scholar]